High spatial resolution in X-ray mapping

Jens Rafaelsen, Tara Nylese
EDAX Inc., 91 McKee Drive, Mahwah, NJ 07430 US

INTRODUCTION

Various microanalysis applications, such as semiconductor and microelectronics, nanotechnology and life sciences, require high resolution analytical performance to understand subtle differences that impact the material's characteristics. The term resolution describes several different aspects of scanning electron microscope (SEM) based microanalysis. In general, it is defined as the ability of the system to resolve, or separate, two aspects of the analysis that are very close together. In imaging and mapping, resolution may be described as the ability to visibly separate two physically closely spaced items. In an X-ray spectrum, it means the ability to differentiate between two elements whose peaks fall at closely spaced energies, as with light element peak separation or low energy x-ray lines.

A common challenge to high resolution microanalysis is the need to reduce the interaction volume of the primary electron beam, which is typically done by reducing the electron energy/SEM acceleration voltage. An estimate of interaction volume can easily be achieved by simulation of the electron trajectories using the CASINO software (1) (2), which also allows the simulation of the spatial distribution of the escaping X-rays as shown in Figure 1 and Figure 2 for a pure silicon sample. If the X-ray resolution in an X-Y-Z coordinate system is considered, Figure 1 clearly shows a dramatic increase in X-ray surface sensitivity with decreasing electron energy thus that the depth/Z resolution is defined by the acceleration voltage. However, Figure 2 indicates that the electron energy only plays a minor role in the X-Y resolution, and that the resolution is largely defined by the size of the electron beam impinging on the sample. This poses a significant challenge for high resolution X-ray imaging since reduced acceleration energy typically results in a larger probe diameter for the same probe current (3). To further complicate matters, lower electron energy also results in lower X-ray yield making it desirable to increase the probe current which again will increase the probe diameter.

With this in mind, high resolution X-ray imaging can be said to involve two primary compromises, the first being between the desired depth resolution and the available X-ray lines, which will define the SEM acceleration voltage.

The second compromise is between the desired X-Y resolution and the probe size/current and consequently the time needed to obtain an acceptable signal-to-noise ratio in the acquired image. One should also keep in mind that the signal-to-noise ratio and good detector resolution plays a larger role for low electron energy spectra compared to high electron energy spectra, since the spectral range and available X-ray lines are limited and deconvolution consequently becomes more complicated.

MATERIALS AND METHODS

Modern semiconductor devices typically include several metal layers, connectors, dielectrics and barrier layers of varying sizes and thus make excellent samples for high resolution mapping. The data presented here was acquired from an Altera Cyclone III FPGA chip. The chip was cross sectioned through the silicon die and then mounted in a copper based conductive mounting powder using a compressive mounting press.

Due to the mounting technique, several large fractures through the silicon die and encapsulation material were observed, though this is of little consequence to the results presented here. After mounting, grinding was performed using 240-, 320-, 400-, 600-, 800-, and 1200-grit SiC abrasive papers, which was followed by polishing using 1.0 micron and 0.3 micron alumina suspensions. Finally a carbon film was deposited using a rod type carbon coater. The cross section was imaged in a JEOL 7000 field emission microscope equipped with an EDAX Octane Plus detector (30 mm^2 active area) and a FEI 200 Nova NanoLab Dualbeam microscope. The Nova microscope was equipped with an EDAX Octane Super

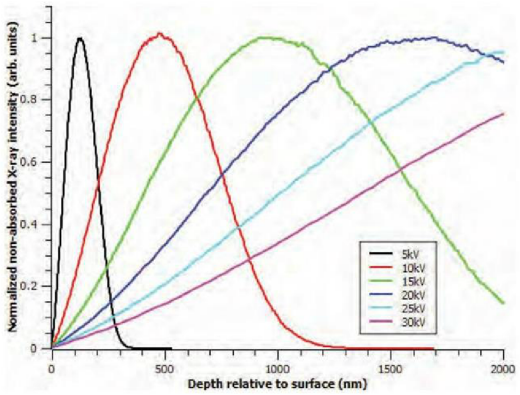

FIGURE 1 Simulation of depth distribution of non-absorbed X-ray intensity at difference acceleration voltages. Simulations were run in CASINO using a beam diameter of 10 nm

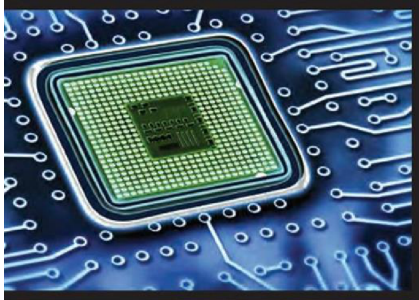

ELEMENT
EDS

The New Element SDD: Fast and Efficient Results

The Element Silicon Drift Detector (SDD) is designed to benefit a wide spectrum of industries such as natural resources and energy, automotive and aerospace, pharmaceutical, steel, and semiconductor.

- Application specific, easy-to-use software with touchscreen capabilities
- Highest performance EDS for the bench top SEM market
- Optimized for low energy X-ray transmission to increase the efficiency of light element detection
- Cost-effective, compact design, easily integrated into an industrial environment

AMETEK®
MATERIALS ANALYSIS DIVISION

edax.com

EDAX®
Smart Insight

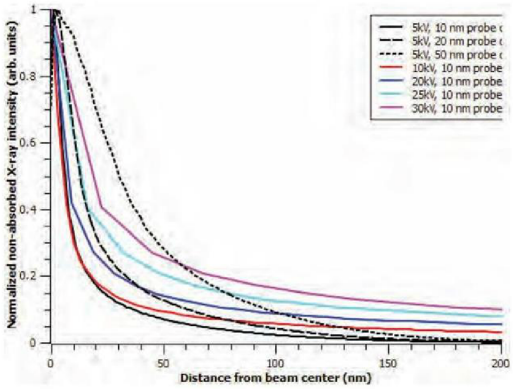

FIGURE 2 Simulation of radial distribution of non-absorbed X-ray intensity at different acceleration voltages and beam diameters. Simulations were run in CASINO

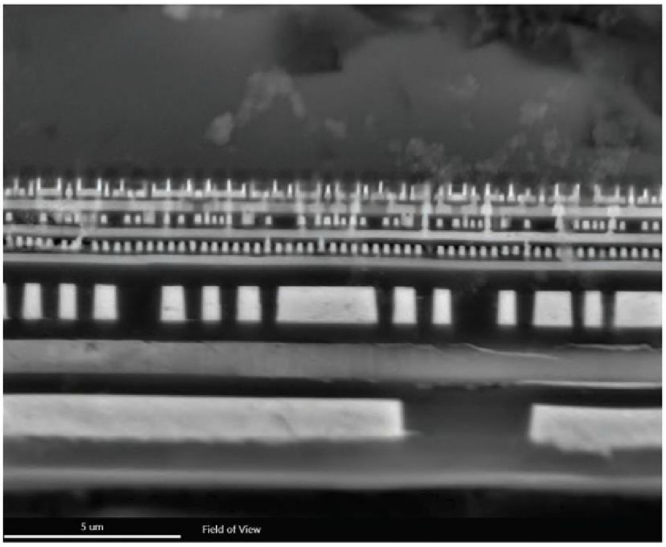

FIGURE 3 SEM secondary electron (SE) image at 20 kV showing an overview of the active region of the Altera Cyclone III FPGA. The encapsulation layer of the device is at the bottom of the image while the Si substrate is at the top

detector (60 mm^2 active area) and an EDAX Octane Pro detector (10 mm^2 active area) with a specialized silicon nitride window as opposed to the traditional polymer windows.

RESULTS

An overview of the device structure can be seen in Figure 3 while Figure 4 and Figure 5 show the Si and combined Cu and W maps respectively. All maps were acquired using an accelerating voltage of 20 keV. The Si substrate shows up bright in the Si map while the slightly darker regions correspond to the SiO_2 dielectric layers in the device. The larger Cu lines are clearly resolved in the Cu map though the fine Cu details of the device close to the substrate is blurred. In contrast to this, the W plugs connecting to the substrate are clearly resolved. Despite the W plugs being better resolved in the map, they are actually smaller than the Cu structures as seen in the SEM image of Figure 6. The reason for this rather counterintuitive result is to be found in the X-ray escape depth of the two materials. While the Cu K and W L X-ray lines are quite close (8.040 and 8.396 keV respectively) the density of W is roughly twice that of Cu and thus the X-ray stopping power is much larger. This means that for the Cu lines the probe depth is actually larger than the size of the structure itself, while the numbers are comparable for the W plugs.

Reducing the accelerating voltage to 10 kV means that the Cu K and W L lines will be poorly excited and so it is necessary to use the W M line at 1.774 and the Cu L line at 0.930 keV for mapping. The reduction in acceleration voltage results in more shallow electron penetration into the sample, but since low energy X-ray lines are more readily absorbed, the use of the Cu L and W M lines also help us confine the analysis volume to the surface. The Si, Cu, and W maps collected at 10 kV of the region in Figure 6 are shown in Figure 7, Figure 8, and Figure 9 respectively. Both the Si and Cu maps show a higher degree of detail than seen in the 20 kV and the W plugs are clearly resolved in the W map. Under the assumptions that the electron beam is Gaussian in shape and that there is a sharp transition between the Cu lines and the surrounding material in the device, the spatial resolution of the image can be calculated based on a line profile through the Cu lines. The line profiles were extracted using ImageJ (4) and the data smoothed with a 20 point adjacent averaging followed by differentiation and fitting with a Gaussian curve. This resulted in an estimated spatial resolution for the Cu map of roughly 60 nm. Corresponding results on 5 kV maps yielded values of roughly 80-100 nm for comparable beam currents, suggesting 10 kV to be the better compromise regarding spatial resolution for the given microscope and sample. Though the estimated resolution is on the order of 60 nm based on the Cu lines, this does not mean that we cannot see smaller structures, as the Ni map of Figure 10 illustrates. Here the nickel silicide layer is clearly seen with a total width of approximately 50 nm.

One thing to note in Figure 9 is that the W map also shows presence of W in the Si substrate. This is one of the issues which we typically encounter when analysing low energy spectra and it stems from the partial overlap of the W M line at 1.774 and the Si K line at 1.740 keV. A similar effect is seen between Ni and Cu in Figure 10. Detector resolutions are often in the range of 70-80 eV in this low energy range, which means that direct separation of the peaks is not possible and we must incorporate a routine to deconvolute the peaks for each spectrum in the map. As long as there are high count numbers and good statistics in the spectra this can be performed routinely, however, the average counts per pixel in a map is typically quite low, making deconvolution a challenge. Of course the simple answer would be to increase the number of X-rays generated by increasing the current, but this is in conflict with our desire to have a small probe size and good X-Y resolution. The other options would be to increase the acquisition time and build up more statistics or use a large active area detector to capture a larger number of generated X-rays.

While low energy spectrum collection and mapping traditionally has been the realm of large active area detectors, size isn't everything. The maps presented here have primarily been collected with a 10 mm^2 active area detector and though a larger area detector would have been able to reach the same average counts per pixel in a shorter amount of time, this particular detector has a few tricks up its sleeve. By using an extremely thin silicon nitride window instead of the traditional polymer one, absorption can be reduced significantly. This gives an overall increase in the throughput relative to a polymer window, but particularly in the low energy range, dramatic increases can be seen. An illustration of this can be seen in the N map shown in Figure 11 where the nitrogen rich layers are clearly resolved, and due to the reduced absorption even Si L lines at 90 eV can now be used for mapping as shown in

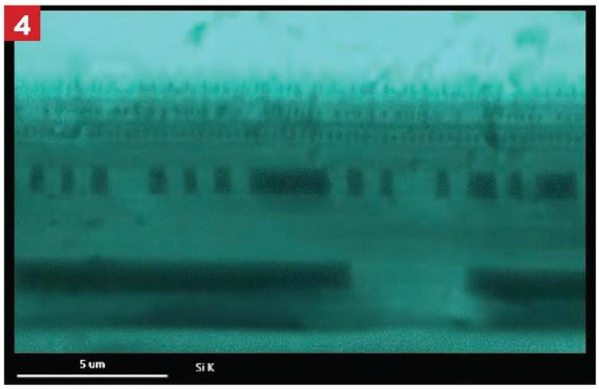

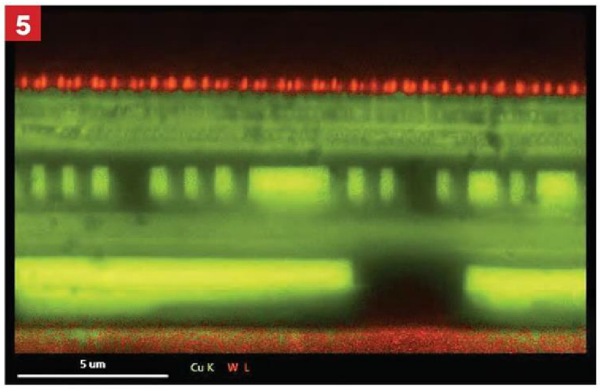

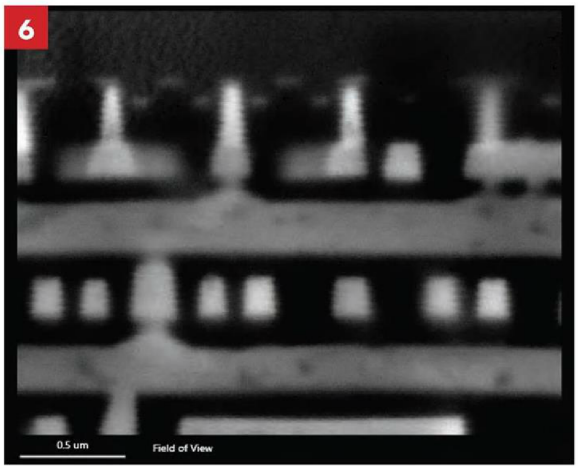

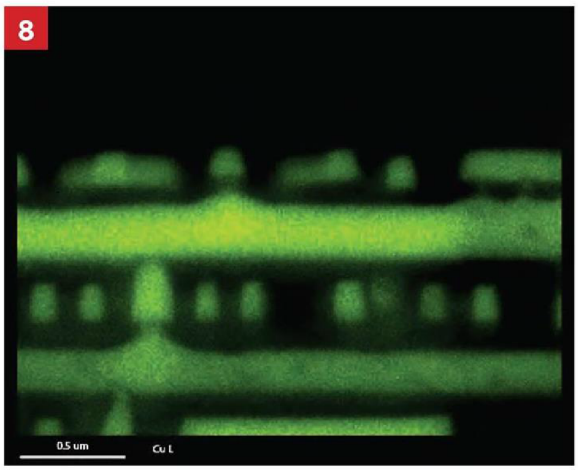

FIGURE 4 Si map of the region shown in Figure 3

FIGURE 5 Cu and W map of the region shown in Figure 3

FIGURE 6 SEM SE image of the Si substrate interface

FIGURE 7 Si map of the region shown in Figure 6

FIGURE 8 Cu map of the region shown in Figure 6

FIGURE 9 W map of the region shown in Figure 6

AM

Figure 12. Despite the challenges with overlaps for the extreme low energy range of X-ray spectra, the detection of the low energy lines opens the door to pushing X-ray microanalysis in the SEM even further towards being a truly surface sensitive technique.

SUMMARY AND CONCLUSIONS

To achieve high spatial resolution in X-ray mapping, it is a necessity to reduce the electron energy/acceleration voltage to limit the X-ray interaction volume and achieve high surface sensitivity. A reduction in acceleration voltage leads to fewer X-rays being generated but while it is tempting to increase the beam current to compensate for the lower yield, the associated increase in beam diameter is detrimental to the mapping resolution. A silicon nitride window increases the yield without the drawbacks of the increased beam current and shows promise for low energy x-ray and high spatial resolution data collection. As with many other aspects of X-ray analysis, a compromise must be made between speed and quality of the data, but modelling of the X-ray distributions can be a strong tool and work as a guideline as to which compromise is the more desirable.

REFERENCES

1 *Casino - monte carlo simulation of electron trajectory in solids.* Université de Sherbrooke. [Online] http://www.gel.usherbrooke.ca/casino/index.html.

2 CASINO V2.42—*A Fast and Easy-to-use Modeling Tool for Scanning Electron Microscopy and Microanalysis Users.*, Dominique Drouin *et al.* 3, s.l. : Scanning, 2007, Vol. 29.

3 J. Goldstein *et al.*, *Scanning Electron Microscopy and X-Ray Microanalysis.* New York : Plenum Press, 1981. ISBN 0-306-40768-X.

4 ImageJ. National Institutes of Health. [Online] http://imagej.nih.gov/ij/.

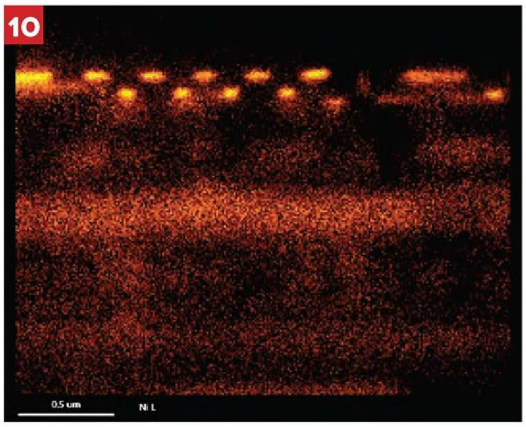

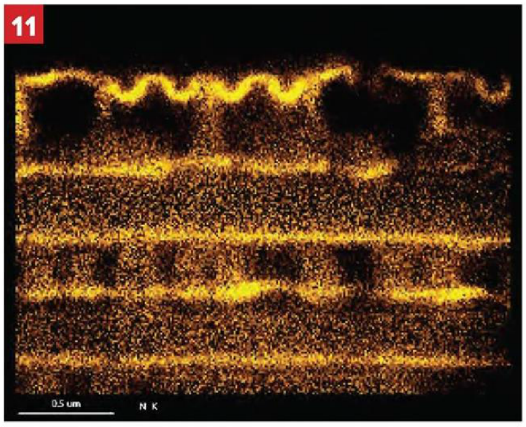

FIGURE 10 Ni map of the region shown in Figure 6

FIGURE 11 N map of the region shown in Figure 6

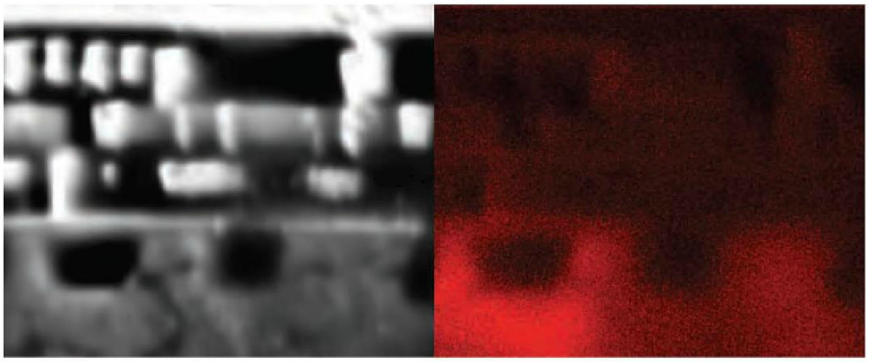

FIGURE 12 SEM image and corresponding Si L line map

BIOGRAPHY

Jens Rafaelsen joined EDAX in 2014 as an Applications Engineer specializing in EDS. He has a strong background in electron microscopy and has trained numerous students and clients in SEM and EDS theory and practice. His experience includes several years as the technical supervisor of the clean room facilities at Aalborg University, Denmark, where he applied a variety of techniques including SEM, FIB, CVD, PVD, PES, AFM, laser spectroscopy, and optical, electron, and ion beam lithography.

Jens earned his PhD in Physics from Aalborg University. His research focused on Germanium surfaces and nanostructures probed by non-linear optical measurement techniques, photoemission spectroscopy, and electron microscopy.

ABSTRACT

In this article we will consider the effects that define the spatial resolution of X-ray mapping using EDS detectors. Using modelling of electron trajectories and X-ray generation, the role of the electron energy and probe size is examined, leading to identification of the primary parameters to consider for high spatial resolution data acquisition. As an example, multiple maps from an Altera Cyclone III FPGA chip are presented and the resolution is assessed.

CORRESPONDING AUTHOR

DETAILS

Jens.rafaelsen@ametek.com

Microscopy and Analysis 29(3): 20-24 (AM), May 2015

©2015 John Wiley and Sons Ltd.